

Cross-Spectrum Measurement Statistics: Uncertainties and Detection Limit

Antoine Baudiquez¹, Graduate Student Member, IEEE, Éric Lantz¹,
 Enrico Rubiola¹, Member, IEEE, and François Vernotte¹

Abstract—The cross-spectrum method consists in measuring a signal $c(t)$ simultaneously with two independent instruments. Each of these instruments contributes to the global noise by its intrinsic (white) noise, whereas the signal $c(t)$ that we want to characterize could be a (red) noise. We first define the real part of the cross spectrum as a relevant estimator. Then, we characterize the probability density function (pdf) of this estimator knowing the noise level (direct problem) as a Variance-gamma (VG) distribution. Next, we solve the “inverse problem” due to Bayes’ theorem to obtain an upper limit of the noise level knowing the estimate. Checked by massive Monte Carlo simulations, VG proves to be perfectly reliable for any number of degrees of freedom (DOFs). Finally, we compare this method with another method using the Karhunen–Loève transform (KLT). We find an upper limit of the signal level slightly different as the one of VG since KLT better considers the available information.

Index Terms—Bayesian statistics, confidence interval, cross spectrum, Karhunen–Loève transform (KLT), probability density function (pdf).

I. INTRODUCTION

THE measurement of power spectra is a classical problem, ubiquitous in numerous branches of physics, as explained next. Power spectra are efficiently measured using Fourier transform (FT) methods with digitized data. Relevant bibliography is now found in classic books [1]–[4].

We are interested in the measurement of weak statistical phenomena, which challenge the instruments and the

mathematical tools, using the cross-spectrum method. This method consists of the simultaneous measurement of the signal with two separate and independent instruments [5]. The other approach, consisting on the observation of the spectral contrast in a chopped signal, broadly equivalent to the Dicke radiometer [6], is not considered here. Regarding the duration of the data record used to evaluate the fast Fourier transform (FFT), two asymptotic cases arise.

The first case is that of the measurement of fast phenomena, where a large number of records denoted m is possible in a reasonable observation time. At large m , the central limit theorem rules and the background noise can be rejected by a factor approximately equal to $1/\sqrt{m}$, depending on the estimator. Numerous examples are found in the measurement of noise in semiconductors [7], phase noise in oscillators and components [8]–[11], frequency fluctuations and relative intensity noise in lasers [12], [13], electromigration in thin films [14], and so on. Restricting to one bin of the FT, the power spectral density (PSD) integrated over a suitable frequency range is used in radiometry [15], [16], Johnson thermometry [17], and other applications.

The second case is that of slow phenomena, where the fluctuations are very long term or nonergodic. On one hand, the background noise is still rejected as before but with a very low m that can actually be equal to one. On the other hand, the central limit theorem does not apply and the statistical uncertainties are not trivial. This case is of great interest in radio astronomy, where the observations are limited by the available resources and take a long time. For instance, millisecond pulsars (MSPs) can be used as very stable clocks at astronomical distances [18]. The radio pulses’ times of arrival (TOAs) of MSP are affected by numerous physical processes, and one of them is gravitational-wave (GW) perturbations [19], [20]. Red noise originated from GW perturbations in the signal path common to the radio telescopes can be detected [21], [22]. As the analysis of the signals provided by the LIGO/VIRGO interferometers that use cross-correlation methods [23], [24], the Large European Array for Pulsars (LEAP) experiment [25] could use such methods in order to access lower frequencies and observe imperceptible phenomena such as early phases well before the coalescence of black holes or GW of cosmological origin (for example, cosmic strings, inflation, and primordial black holes).

Manuscript received March 16, 2020; accepted June 20, 2020. Date of publication June 29, 2020; date of current version October 26, 2020. This work was supported in part by the ANR Programmes d’Investissement d’Avenir (PIA) Oscillator IMP under Project 11-EQPX-0033 and in part by the Formation, Innovation, Recherche, Services et Transfert en Temps-Fréquence (FIRST-TF) under Project 10-LABX-0048. (Corresponding author: Antoine Baudiquez.)

Antoine Baudiquez is with FEMTO-ST, Department of Time and Frequency, UMR 6174, Université Bourgogne Franche-Comté, 25 030 Besançon, France (e-mail: antoine.baudiquez@femto-st.fr).

Éric Lantz is with FEMTO-ST, Département d’Optique P. M. Duffieux, UMR 6174 CNRS, Université Bourgogne Franche-Comté, 25 030 Besançon, France.

Enrico Rubiola is with FEMTO-ST, Department of Time and Frequency, UMR 6174, Université Bourgogne Franche-Comté, 25000 Besançon, France, and also with the Division of Quantum Metrology and Nanotechnology, Istituto Nazionale di Ricerca Metrologica (INRIM), 10135 Turin, Italy.

François Vernotte is with FEMTO-ST, Department of Time and Frequency, Observatory THETA, UMR 6174 CNRS, Université Bourgogne Franche-Comté, 25 030 Besançon, France.

Digital Object Identifier 10.1109/TUFFC.2020.3005785

This article is intended to put an upper limit on the uncertainty of the cross-spectrum estimate. The method proposed here is totally general regardless of the power law type of noise. Indeed, even if the pulsar signal would be constituted by white noise, the realizations of this white noise would be the same, for low frequency, at different observatories, whereas the realizations of measurement white noise are independent. However, this article shows a particular interest in red noise. GWs have not been yet discovered in the TOA of MSPs. Due to the very long line of sight between the pulsars and us (several thousand light-years), we could access very low frequencies, inaccessible to LIGO/VIRGO, thus revealing much slower astrophysical phenomena. It is therefore important to develop statistical tools to improve measurement sensitivity to pulsar timing observations [26]. In this respect, we propose in Section II to state the cross-spectrum problem to define a proper estimate. Based on the principle that the experiment is repeated m times, it is important to note that the estimation of the measurement uncertainty is A-Type as defined by the VIM [27]. Then, in Section III, we define the probability density function (pdf) (i.e., “direct problem”) of the cross-spectrum estimate, which is used in Section IV to compute an upper limit by using a Bayesian inference approach (i.e., “inverse problem”). The results obtained are compared with another method using the Karhunen–Loève transform (KLT) developed in [28] and the conclusions are presented in Section V.

II. STATEMENT OF THE PROBLEM

A. Spectral Measurement

This article aims to measure the mathematical expectation of the amplitude for a frequency bin. This amplitude obviously depends on the frequency and this is what we are looking for, as shown in Fig. 1. Let us remind that the FT of white noise is a white noise. FT, random signals have generally infinite energy, so the real FT cannot be generally defined. A description of a realistic white noise actually corresponds to a Markov process of the first order and the reader can report to [29] for discrete simulation of colored noise and stochastic processes. The random part of the amplitude of each frequency bin is then uncorrelated from each bin. Considering a red noise as a filtered white noise means that the red noise spectrum is the product of the white spectrum by a deterministic function and, therefore, the uncorrelation property of the random part of the red noise spectrum is preserved. Working directly in the frequency domain, therefore, changes absolutely nothing in terms of a random variable. Consequently, it does not matter to know whether the signals are stationary, uncorrelated, or not since we are interested in the spectrum and in a bin of frequency in particular.

B. Cross-Spectrum Method

Let us consider three statistically independent signals, $a(t)$, $b(t)$, and $c(t)$, as shown in Fig. 2. On one side, the two first $a(t)$ and $b(t)$ are, respectively, the instrument noise of \mathcal{A} and \mathcal{B} . On the other side, $c(t)$ is an input signal that we want to characterize. This signal is stochastic and not necessarily

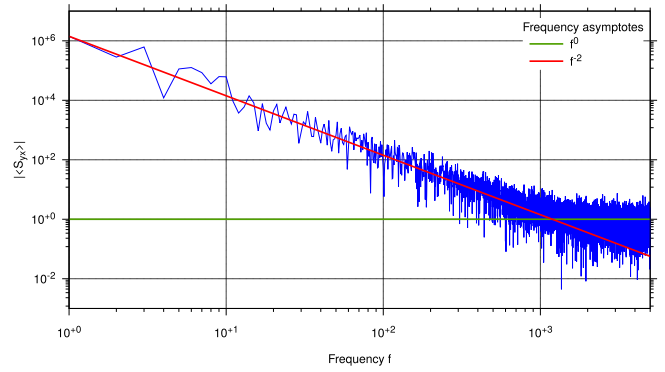


Fig. 1. PSD estimate magnitude obtained via a discrete FT. The red and green dashed lines correspond to the power-law frequency asymptotes related to the signal.

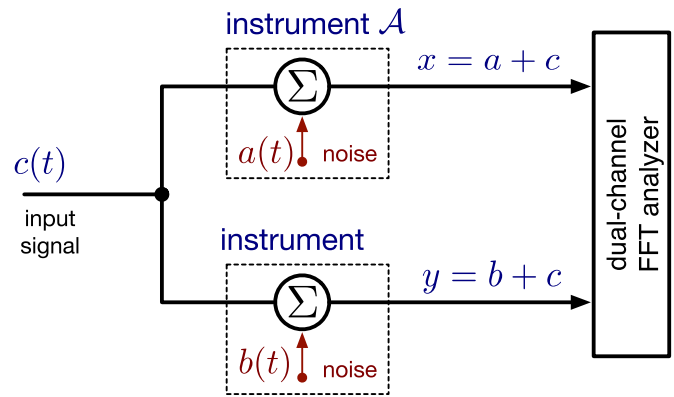


Fig. 2. Basics of the cross-spectrum method.

stationary. In the case of pulsar measurement, this input signal is generally a red noise. The output of each channel is

$$\begin{aligned} x(t) &= a(t) + c(t) \\ y(t) &= b(t) + c(t). \end{aligned} \quad (1)$$

Processing experimental signals, we can assume that white noise is a continuous function of time and that the FT always exists if we look at a very short interval regarding the sampling period. The reader can refer to [30] for a more detailed model of realistic white noise. Applying the FT on each channel gives

$$\begin{aligned} X(f) &= A(f) + C(f) \\ Y(f) &= B(f) + C(f) \end{aligned} \quad (2)$$

where f is the frequency, $X(f)$, $Y(f)$, $A(f)$, $B(f)$, and $C(f)$ stand, respectively, for the FT of $x(t)$, $y(t)$, $a(t)$, $b(t)$, and $c(t)$. Our interest is carried out on the PSD rather than the spectrum. The cross spectrum is defined as

$$S_{yx}(f) = \frac{1}{T} \mathbb{E}[Y(f)X^*(f)] \quad (3)$$

where the cross-spectrum is actually a cross-PSD and $\mathbb{E}[\cdot]$ stands for the mathematical expectation of the quantity within the brackets. The factor T is the measurement time, which is necessary for because the power calculated in time domain and in frequency domain must be the same (Parseval theorem) and

also for $S_{yx}(f)$ to have the dimension of power per unit of frequency. * denotes the complex conjugate of the quantity placed before it. Equation 3 is the two-side PSD, which contains positive and negative frequencies. Experimentally averaging over m spectra realizations leads to the following cross-PSD estimator:

$$\langle S_{yx} \rangle_m = \frac{1}{T} \langle Y(f)X^*(f) \rangle_m. \quad (4)$$

C. Cross Power Spectral Density

Averaging on a large number of observations, the mathematics is made simple by the central limit theorem, by which all the pdfs become Gaussian. More interesting for us is the case of a small number of realizations, each of which taking long observation time-up to several years in the case of the MSPs.

The random variables (rv) $a(t)$, $b(t)$, and $c(t)$ follow a centered normal distribution whatever the kind of noise. Even red noise (e.g., random walk) follows a normal distribution not on the time average but regarding its ensemble average over the probability space, meaning that it is a nonergodic process. Moreover, a stochastic process with zero-mean Gaussian distribution has an FT, which is also a random process with centered Gaussian distribution.

rv $A(f)$, $B(f)$, and $C(f)$ can then be decomposed into a real and imaginary parts

$$\begin{aligned} A(f) &= A'(f) + iA''(f) \\ B(f) &= B'(f) + iB''(f) \\ C(f) &= C'(f) + iC''(f). \end{aligned} \quad (5)$$

The real and imaginary parts are statistically independent rv with equal variance following a zero-mean Gaussian distribution. For an ensemble average or a time sequence sufficiently long to ensure a good spectral resolution, the samples at different frequencies are independent of each other. Hence, all the results of this article are given for a given frequency that we do not mention explicitly. Of course, there is a deterministic relation between the results and this frequency, except in the case of a signal constituted by white noise, which is not the most common assumption in the envisioned applications. Let us now expand (4)

$$\begin{aligned} \langle S_{yx} \rangle_m &= \frac{1}{T} \langle YX^* \rangle_m \\ &= \frac{1}{T} [\langle A'B' + B'C' + C'A' + C'^2 \rangle_m \\ &\quad + \langle A''B'' + B''C'' + C''A'' + C''^2 \rangle_m \\ &\quad + i \langle A'B'' + B''C' + C''A' \rangle_m \\ &\quad - i \langle A''B' + B'C'' + C'A'' \rangle_m]. \end{aligned} \quad (6)$$

The terms in the imaginary part have a zero expectation, whereas the expectation in the real part is proportional to the PSD of the signal, i.e., what we are looking to characterize. As a consequence, Sections III and IV focus solely on the real part $\Re\{S_{yx}\}$

$$\langle \Re\{S_{yx}\} \rangle_m = \frac{1}{T} \langle (A^k + C^k)(B^k + C^k) \rangle_\nu \quad (7)$$

where $\nu = 2m$ the number of degree of freedom (DOF). The superscript k means real or imaginary part because they are independent rv.

D. Statement of the Problem

1) *Measurements and Estimates*: In the following, in order to simplify the notation, we will omit the superscript k . Thereby, the real and imaginary parts will be treated as two DOFs. Moreover, to simplify the notations, we will omit the factor $1/T$, which does not affect the pdf. The estimates will be noted with a “hat” and we refer the cross-spectrum measurement for a given frequency to

$$\hat{Z} = (\hat{A} + \hat{C})(\hat{B} + \hat{C}) \quad (8)$$

where all \hat{A} , \hat{B} , and \hat{C} are rv which are independent, centered, and normal. In the following, we will assume that \hat{A} , \hat{B} , and \hat{C} have only one DOF, their real or their imaginary part, and that \hat{Z} does not come from the average of different spectra. A generalization of this problem to two DOFs (real and imaginary parts) and then $2m$ DOF (average of m spectra) will be given.

2) *Direct and Inverse Problem*: In order to assess the uncertainty over the estimator σ_C^2 , called the signal level, we will have to distinguish to main issues.

- 1) The direct problem consists in calculating the statistics of the cross-spectrum measurement \hat{Z} , knowing the model parameters σ_A^2 , σ_B^2 , and σ_C^2 .
- 2) The inverse problem conversely consists in calculating a confidence interval over the unknown model parameter σ_C^2 , from the known parameters σ_A^2 and σ_B^2 and the cross-spectrum measurement \hat{Z} .

III. DIRECT PROBLEM

In Sections III-A–III-E, we will omit the “hat” for estimates since we deal with the mathematical models.

A. Vector Formalization of the Problem

We will reuse here the formalism we developed in [31], i.e., a vector space of normal laws. Since we have three normal rv, we are in a vector space of three dimensions that we will denote $\mathbb{L}\mathbb{G}^3$, which has the basis $(\vec{E}_A, \vec{E}_B, \vec{E}_C)$ defined as

$$\begin{cases} \vec{E}_A = \text{LG}_A(0, 1) \\ \vec{E}_B = \text{LG}_B(0, 1) \\ \vec{E}_C = \text{LG}_C(0, 1) \end{cases}$$

where $\text{LG}(0, 1)$ stands for a Laplace–Gauss (or normal) rv with zero-mean (centered) and unity standard deviation ($\sigma = 1$). We assume that $\text{LG}_A(0, 1)$, $\text{LG}_B(0, 1)$, and $\text{LG}_C(0, 1)$ are independent. We can define the scalar product between the basis vectors of $\mathbb{L}\mathbb{G}^3$ in such a way

$$\begin{cases} \|\vec{E}_A\|^2 = \vec{E}_A \cdot \vec{E}_A = \text{LG}_A \cdot \text{LG}_A = \chi_A^2 \\ \|\vec{E}_B\|^2 = \vec{E}_B \cdot \vec{E}_B = \text{LG}_B \cdot \text{LG}_B = \chi_B^2 \\ \|\vec{E}_C\|^2 = \vec{E}_C \cdot \vec{E}_C = \text{LG}_C \cdot \text{LG}_C = \chi_C^2 \\ \vec{E}_A \cdot \vec{E}_B = \text{LG}_A \cdot \text{LG}_B = \text{V}\Gamma_{AB} \\ \vec{E}_B \cdot \vec{E}_C = \text{LG}_B \cdot \text{LG}_C = \text{V}\Gamma_{BC} \\ \vec{E}_C \cdot \vec{E}_A = \text{LG}_C \cdot \text{LG}_A = \text{V}\Gamma_{CA} \end{cases}$$

where $\chi_{A,B,C}^2$ are three independent χ^2 rv with one DOF and $\mathbf{V}\Gamma_{AB,BC,CA}$ are three VD rv [31], [32]. Any vector \vec{U} may be written as

$$\vec{U} = \begin{pmatrix} u_A \\ u_B \\ u_C \end{pmatrix} = u_A \vec{E}_A + u_B \vec{E}_B + u_C \vec{E}_C$$

where u_A, u_B , and u_C are three constant scalars since all the random part is carried by the basis vectors. The scalar product between two vectors \vec{U} and \vec{V} is then

$$\begin{aligned} \vec{U} \cdot \vec{V} &= (u_A \vec{E}_A + u_B \vec{E}_B + u_C \vec{E}_C) \\ &\quad \cdot (v_A \vec{E}_A + v_B \vec{E}_B + v_C \vec{E}_C) \\ &= u_A v_A \vec{E}_A \cdot \vec{E}_A + u_B v_B \vec{E}_B \cdot \vec{E}_B + u_C v_C \vec{E}_C \cdot \vec{E}_C \\ &\quad + (u_A v_B + u_B v_A) \vec{E}_A \cdot \vec{E}_B \\ &\quad + (u_B v_C + u_C v_B) \vec{E}_B \cdot \vec{E}_C \\ &\quad + (u_C v_A + u_A v_C) \vec{E}_C \cdot \vec{E}_A. \end{aligned}$$

On the other hand, if we consider the mathematical expectation of these expressions, we obtain

$$\mathbb{E}[\vec{E}_P \cdot \vec{E}_Q] = \delta_{P,Q} \quad \text{with } P, Q \in \{A, B, C\}$$

where $\delta_{P,Q}$ is the Kronecker delta. We see that we obtain the classical scalar product by using the mathematical expectation

$$\mathbb{E}[\vec{U} \cdot \vec{V}] = u_A v_A + u_B v_B + u_C v_C.$$

Therefore, we will define that two vectors \vec{U} and \vec{V} are orthogonal if $\mathbb{E}[\vec{U} \cdot \vec{V}] = 0$.

B. From a Normal Random Variable Product to a Chi-Squared RV Difference

Following this formalism, (8) may be rewritten as

$$\begin{aligned} Z &= (\vec{A} + \vec{C}) \cdot (\vec{B} + \vec{C}) = \begin{pmatrix} a \\ 0 \\ c \end{pmatrix} \cdot \begin{pmatrix} 0 \\ b \\ c \end{pmatrix} \\ &= ab\mathbf{V}\Gamma_{AB} + ac\mathbf{V}\Gamma_{AC} + bc\mathbf{V}\Gamma_{BC} + c^2\chi_C^2 \end{aligned} \quad (9)$$

where a, b , and c are, respectively, the standard deviations of the rv A, B , and C . As a consequence, $\mathbb{E}[Z] = c^2$. In the following, we will use the noise variances $\sigma_A^2 = a^2$ and $\sigma_B^2 = b^2$ and the signal variance $\sigma_C^2 = c^2$.

As demonstrated in [33], a product of independent normal rv may be expressed as a difference of χ^2 rv. For this purpose, although we know that $(A + C)$ and $(B + C)$ are not independent, we introduce the rv $V_1 = (A + B)/2 + C$ and $V_2 = (A - B)/2$ in such a way that $A + C = V_1 + V_2$ and $B + C = V_1 - V_2$, and therefore, $(A + C)(B + C) = V_1^2 - V_2^2$. In this vectorial formalism

$$\vec{V}_1 = \begin{pmatrix} a/2 \\ b/2 \\ c \end{pmatrix}, \quad \text{and } \vec{V}_2 = \begin{pmatrix} a/2 \\ -b/2 \\ 0 \end{pmatrix}.$$

Therefore, (\vec{V}_1, \vec{V}_2) is the basis of the 2-D subspace of $\mathbb{L}\mathbb{G}^3$ in which lies our whole problem. Since the squared modulus

of \vec{V}_1 and \vec{V}_2 are

$$\begin{cases} \|\vec{V}_1\|^2 = \frac{a^2}{4}\chi_A^2 + \frac{b^2}{4}\chi_B^2 + c^2\chi_C^2 \\ + \frac{ab}{2}\mathbf{V}\Gamma_{AB} + ac\mathbf{V}\Gamma_{AC} + bc\mathbf{V}\Gamma_{BC} \\ \|\vec{V}_2\|^2 = \frac{a^2}{4}\chi_A^2 + \frac{b^2}{4}\chi_B^2 - \frac{ab}{2}\mathbf{V}\Gamma_{AB} \end{cases}$$

their difference is consistent with (9), and then, $Z = (\vec{A} + \vec{C}) \cdot (\vec{B} + \vec{C}) = \|\vec{V}_1\|^2 - \|\vec{V}_2\|^2$. Moreover, we can calculate the mathematical expectations of these squared modulus

$$\begin{aligned} v_1^2 &= \mathbb{E}[\|\vec{V}_1\|^2] = \frac{a^2 + b^2}{4} + c^2 \\ v_2^2 &= \mathbb{E}[\|\vec{V}_2\|^2] = \frac{a^2 + b^2}{4}. \end{aligned} \quad (10)$$

On the other hand, since

$$\mathbb{E}[\vec{V}_1 \cdot \vec{V}_2] = \frac{a^2 - b^2}{4} \quad (11)$$

the vector \vec{V}_1 and \vec{V}_2 are not orthogonal unless $a = b$, i.e., A and B have the same variance.

C. Particular Case: A and B Have the Same Variance

Let us define $\sigma_N^2 = \sigma_A^2 = \sigma_B^2 = n^2$, i.e., $n = a = b$. In this case

$$\mathbb{E}[\vec{V}_1 \cdot \vec{V}_2] = \frac{n^2}{4} - \frac{n^2}{4} = 0$$

\vec{V}_1 and \vec{V}_2 are orthogonal, meaning that their squared modulus are two independent χ^2 rv

$$\|\vec{V}_1\|^2 = v_1^2\chi_{v_1}^2 \quad \text{and } \|\vec{V}_2\|^2 = v_2^2\chi_{v_2}^2.$$

Due to [31, Appendix A], we know that this χ^2 rv difference is a $\mathbf{V}\Gamma$ rv with a pdf, introduced by [34]

$$p(x) = \frac{\gamma^{2\lambda} |x - \mu|^{\lambda-1/2} K_{\lambda-1/2}(\alpha|x - \mu|)}{\sqrt{\pi}\Gamma(\lambda)(2\alpha)^{\lambda-1/2}} e^{\beta(x-\mu)} \quad (12)$$

where $\gamma = (\alpha^2 - \beta^2)^{1/2}$, $\Gamma(\lambda)$ is the gamma function, $K_w(z)$ is a hyperbolic Bessel function of the second kind ($w \in \mathbb{R}$ and $z \in \mathbb{C}$) and with the following parameters:

$$\mu = 0, \quad \alpha = \frac{v_1^2 + v_2^2}{4v_1^2v_2^2}, \quad \beta = \frac{v_1^2 - v_2^2}{4v_1^2v_2^2}, \quad \lambda = \frac{1}{2} \quad (13)$$

where λ is the number of DOF divided by 2. In this particular case, since $a^2 = b^2 = n^2$, v_1^2 and v_2^2 become

$$v_1^2 = \mathbb{E}[\|\vec{V}_1\|^2] = \frac{n^2}{2} + c^2 \quad \text{and } v_2^2 = \mathbb{E}[\|\vec{V}_2\|^2] = \frac{n^2}{2},$$

and we obtain

$$\alpha = \frac{n^2 + c^2}{n^2(2n^2 + c^2)} \quad \text{and } \beta = \frac{c^2}{n^2(2n^2 + c^2)}.$$

D. General Case

If $\sigma_A^2 \neq \sigma_B^2$, \vec{V}_1 and \vec{V}_2 are no longer orthogonal and, therefore, they are two correlated rv. We have then to search for another set of orthogonal basis vectors. For this purpose, let us use the Gram–Schmidt process.

1) *Gram–Schmidt Orthogonalization*: Let us keep \vec{V}_1 unchanged. Let \vec{V}_{2P} be the projection of \vec{V}_2 onto \vec{V}_1 . Denoting θ the angle¹ between \vec{V}_1 and \vec{V}_2 , it comes

$$\vec{V}_{2P} = v_2 \cos(\theta) \frac{\vec{V}_1}{v_1}$$

with

$$\cos(\theta) = \frac{\mathbb{E}[\vec{V}_1 \cdot \vec{V}_2]}{v_1 v_2}$$

and then

$$\vec{V}_{2P} = \frac{\mathbb{E}[\vec{V}_1 \cdot \vec{V}_2]}{v_1^2} \vec{V}_1. \quad (14)$$

Therefore, we can build the vector \vec{V}_{2N} that is the component of \vec{V}_2 orthogonal to \vec{V}_1

$$\vec{V}_{2N} = \vec{V}_2 - \vec{V}_{2P} = \vec{V}_2 - \frac{\mathbb{E}[\vec{V}_1 \cdot \vec{V}_2]}{v_1^2} \vec{V}_1.$$

Using (10) and (11) yields

$$\begin{aligned} \vec{V}_{2N} &= \begin{pmatrix} a/2 \\ -b/2 \\ 0 \end{pmatrix} - \frac{a^2 - b^2}{a^2 + b^2 + 4c^2} \begin{pmatrix} a/2 \\ b/2 \\ c \end{pmatrix} \\ &= \begin{pmatrix} \frac{a(b^2 + 2c^2)}{a^2 + b^2 + 4c^2} \\ -\frac{b(a^2 + 2c^2)}{a^2 + b^2 + 4c^2} \\ -\frac{c(a^2 - b^2)}{a^2 + b^2 + 4c^2} \end{pmatrix} = \begin{pmatrix} v_{2nA} \\ v_{2nB} \\ v_{2nC} \end{pmatrix}. \end{aligned}$$

We have now to express the measurement vectors $\vec{A} + \vec{C}$ and $\vec{B} + \vec{C}$ as linear combinations of the new basis of orthogonal vectors \vec{V}_1 and \vec{V}_{2N} . In order to do this, we must project these two measurement vectors onto the two basis vectors in the same way that we have projected \vec{V}_2 onto \vec{V}_1 in (14)

$$\begin{cases} \vec{A} + \vec{C} = k_{AC1} \vec{V}_1 + k_{AC2n} \vec{V}_{2N} \\ \vec{B} + \vec{C} = k_{BC1} \vec{V}_1 + k_{BC2n} \vec{V}_{2N} \end{cases}$$

with

$$\begin{aligned} k_{AC1} &= \frac{\mathbb{E}[(\vec{A} + \vec{C}) \cdot \vec{V}_1]}{\mathbb{E}[\|\vec{V}_1\|^2]} k_{AC2n} = \frac{\mathbb{E}[(\vec{A} + \vec{C}) \cdot \vec{V}_{2N}]}{\mathbb{E}[\|\vec{V}_{2N}\|^2]} \\ k_{BC1} &= \frac{\mathbb{E}[(\vec{B} + \vec{C}) \cdot \vec{V}_1]}{\mathbb{E}[\|\vec{V}_1\|^2]} k_{BC2n} = \frac{\mathbb{E}[(\vec{B} + \vec{C}) \cdot \vec{V}_{2N}]}{\mathbb{E}[\|\vec{V}_{2N}\|^2]}. \end{aligned}$$

Therefore, $Z = (\vec{A} + \vec{C}) \cdot (\vec{B} + \vec{C})$ may be written as

$$\begin{aligned} Z &= k_{AC1} k_{BC1} \|\vec{V}_1\|^2 + k_{AC2n} k_{BC2n} \|\vec{V}_{2N}\|^2 \\ &\quad + (k_{AC1} k_{BC2n} + k_{AC2n} k_{BC1}) \vec{V}_1 \cdot \vec{V}_{2N} \\ &= k_{AC1} k_{BC1} \check{\chi}^2 + k_{AC2n} k_{BC2n} \check{\chi}^2 \\ &\quad + (k_{AC1} k_{BC2n} + k_{AC2n} k_{BC1}) \text{V}\Gamma \end{aligned} \quad (15)$$

¹In the same way as the orthogonality between two vectors is defined by the null mathematical expectation of their scalar product, the angles as well as the other relationships between vectors must be considered as mathematical expectation since they are valid on average but not for only one particular realization of these vectors.

where $\check{\chi}^2$ and $\check{\chi}^2$ are independent χ^2 rv corresponding, respectively, to the squared norm of \vec{V}_1 and \vec{V}_{2N} . Thus, this relationship involves the difference of 2 χ^2 rv (it can be proved that $k_{AC2n} k_{BC2n} < 0$), which is well known [31], [33], plus a $\text{V}\Gamma$ rv, which makes the problem more complex. In order to simplify this problem, we should find a representation of (15) in which the cross term is identically null.

2) *Normalization and Rotation of the Basis Vectors*: Let (\vec{V}'_1, \vec{V}'_2) be the normalized equivalent of the basis $(\vec{V}_1, \vec{V}_{2N})$

$$\vec{V}'_1 = \frac{\vec{V}_1}{\mathbb{E}[\|\vec{V}_1\|]} \quad \text{and} \quad \vec{V}'_2 = \frac{\vec{V}_{2N}}{\mathbb{E}[\|\vec{V}_{2N}\|]}.$$

With this new basis, (15) may be rewritten as

$$\begin{aligned} Z &= k_{AC1} k_{BC1} \mathbb{E}[\|\vec{V}_1\|]^2 \|\vec{V}'_1\|^2 \\ &\quad + k_{AC2n} k_{BC2n} \mathbb{E}[\|\vec{V}_{2N}\|]^2 \|\vec{V}'_2\|^2 \\ &\quad + k_{AC1} k_{BC2n} \mathbb{E}[\|\vec{V}_1\|] \mathbb{E}[\|\vec{V}_{2N}\|] \vec{V}'_1 \cdot \vec{V}'_2 \\ &\quad + k_{AC2n} k_{BC1} \mathbb{E}[\|\vec{V}_1\|] \mathbb{E}[\|\vec{V}_{2N}\|] \vec{V}'_1 \cdot \vec{V}'_2 \\ &= k'_{11} \|\vec{V}'_1\|^2 - k'_{22} \|\vec{V}'_2\|^2 + k'_{12} \vec{V}'_1 \cdot \vec{V}'_2 \end{aligned} \quad (16)$$

with

$$\begin{cases} k'_{11} = k_{AC1} k_{BC1} \mathbb{E}[\|\vec{V}_1\|]^2 \\ k'_{22} = -k_{AC2n} k_{BC2n} \mathbb{E}[\|\vec{V}_{2N}\|]^2 \\ k'_{12} = k_{AC1} k_{BC2n} \mathbb{E}[\|\vec{V}_1\|] \mathbb{E}[\|\vec{V}_{2N}\|] \\ \quad + k_{AC2n} k_{BC1} \mathbb{E}[\|\vec{V}_1\|] \mathbb{E}[\|\vec{V}_{2N}\|]. \end{cases}$$

We can then consider (16) as the expression of a quadratic form Q which associates a scalar w_0 to any vector $\vec{W} = w_1 \vec{V}'_1 + w_2 \vec{V}'_2$. Such a quadratic form may be described as

$$w_0 = \vec{w}^T [Q] \vec{w} \quad \text{with} \quad [Q] = \begin{pmatrix} k'_{11} & k'_{12}/2 \\ k'_{12}/2 & -k'_{22} \end{pmatrix}. \quad (17)$$

The simplification of our problem relies then on a rotation of the basis vectors in such a way that the quadratic form matrix $[Q]$ is diagonal. The eigenvalues of $[Q]$ are given by

$$\ell_1 = \frac{k'_{11} - k'_{22} - \sqrt{\Delta}}{2} \quad \text{and} \quad \ell_2 = \frac{k'_{11} - k'_{22} + \sqrt{\Delta}}{2}$$

with $\Delta = (k'_{11} + k'_{22})^2 + k'_{12}{}^2$. Due to this rotation of the basis vectors, (15) and (16) become

$$Z = \ell_1 \check{\chi}^2 + \ell_2 \check{\chi}^2.$$

As already stated in Section III-C, Z is a $\text{V}\Gamma$ rv with the following pdf parameters:

$$\mu = 0, \quad \alpha = \frac{\ell_1^2 + \ell_2^2}{4\ell_1^2 \ell_2^2}, \quad \beta = \frac{\ell_1 - \ell_2}{4\ell_1^2 \ell_2^2}, \quad \lambda = \frac{1}{2}. \quad (18)$$

E. Generalization to Larger Degrees of Freedom

In the case of $2m$ DOF, i.e., real part + imaginary part multiplied by m averaged uncorrelated spectra, the only change to apply concerns the parameter λ in (13) and (18), which becomes $\lambda = m$.

According to [35, eq. (12), p. 80], we have the following relation:

$$K_{n+\frac{1}{2}}(z) = \left(\frac{\pi}{2z}\right)^{\frac{1}{2}} e^{-z} \sum_{r=0}^n \frac{(n+r)!}{r!(n-r)!(2z)^r} \quad (19)$$

with $n \in \mathbb{N}$ and $z \in \mathbb{C}$. Moreover, $m \in \mathbb{N}^*$, which leads to the relation $n = m - 1$. Therefore, let us expand (12) using (19)

$$p(x) = \frac{\kappa(\alpha, \beta)^m \epsilon(x, \mu, \alpha, m)}{\Gamma(m)} e^{-\alpha|x-\mu|+\beta(x-\mu)} \quad (20)$$

with the following parameters:

$$\kappa(\alpha, \beta) = \frac{\alpha^2 - \beta^2}{2\alpha} \quad \Gamma(m) = (m-1)!$$

$$\epsilon(x, \mu, \alpha, m) = \sum_{r=0}^{m-1} \frac{(m+r-1)! |x-\mu|^{m-r-1}}{r!(m-r-1)!(2\alpha)^r}.$$

F. Validation of the Theoretical Probability Laws by Monte Carlo Simulations

1) *Algorithm Description*: According to Section III-D2, the probability density of \hat{Z} , equal to the difference of two independent χ^2 rv, can now be calculated using the function $p(x)$ of (20) by assigning the values to the parameters in (13) and (18). In order to perform this comparison, we use two algorithms, one for Monte Carlo (MC) simulation and the other one for computing (20).

a) *MC simulation algorithm*: The simulation algorithm follows these six steps.

- S1: Assignment of the two noise levels σ_A^2 and σ_B^2 , signal level σ_C^2 , and the number of averaging spectra m .
- S2: Drawing of \hat{A} , \hat{B} , and \hat{C} , following a normal centered distribution with, respectively, σ_A , σ_B , and σ_C as standard deviation.
- S3: Computation of $\hat{Z} = (\hat{A} + \hat{C})(\hat{B} + \hat{C})$.
- S4: Repetition $2m$ times of steps S2 to S3 and sum all \hat{Z} values.
- S5: Repetition $N = 10^7$ times of steps S2 to S4 of this sequence.
- S6: Drawing the histogram of \hat{Z} .

In all simulations, we chose a number of DOFs $\nu = 2m$ in order to have the real and imaginary parts in agreement with the experiment shown in Fig. 2.

b) *Modeling algorithm*: The modeling algorithm follows also six steps.

- S1: Assignment of the two noise levels σ_A^2 and σ_B^2 , signal level σ_C^2 , and the number of averaging spectra m .
- S2: *Independent basis*:
 - a) Computation of coefficients v_1^2 and v_2^2 according to (10).

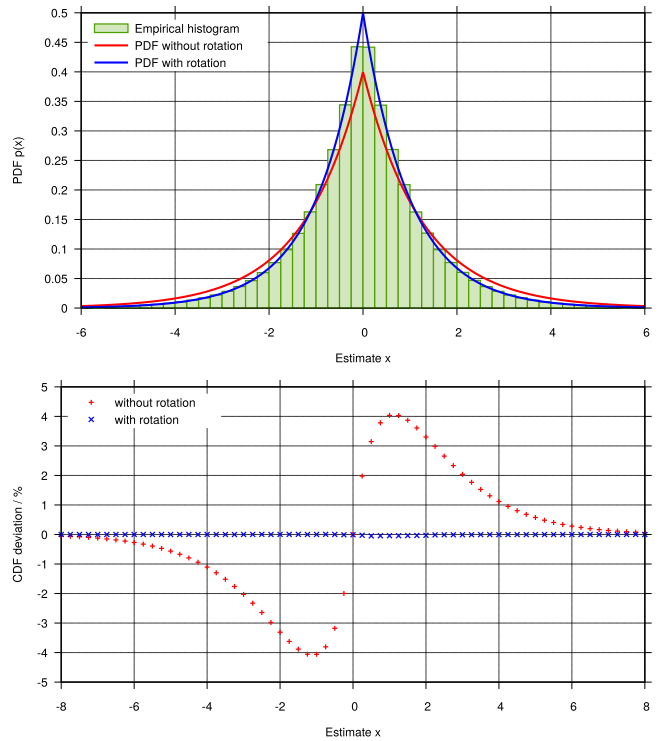


Fig. 3. Comparison of the empirical and theoretical pdf (above) with and without rotation of the basis vectors. The deviations between the empirical and the theoretical CDF are given in the bottom. The variances are: $\sigma_C^2 = 0$, $\sigma_A^2 = 2$, and $\sigma_B^2 = 1/2$ and there are two DOFs.

- b) If $\sigma_A^2 = \sigma_B^2$, go to step S5; else, perform steps S3 and S4

S3: *Orthogonalization of the Basis*:

- a) computation of coefficients k_{AC1} , k_{AC2n} , k_{BC1} , and k_{BC2n} to determine the new basis according to (15);
- b) normalization of the basis by determining coefficients k'_{11} , k'_{22} , and k'_{12} according to (16).

S4: *Vector Rotation*:

- a) diagonalization of the matrix Q according to (17);
- b) computation of its roots l_1 and l_2 .

S5: Compute the coefficients α , β , and $\lambda = m$ according to (13) and (18).

S6: Plotting the probability density with (20).

2) *When Can the Instrument Noises Be Assumed to Be "About the Same"?*: Although the problem is quite simple when the instrument noises σ_A^2 and σ_B^2 are the same (see Section III-C), it becomes more complex when $\sigma_A^2 \neq \sigma_B^2$. The question is then how far can we assume that $\sigma_A^2 \approx \sigma_B^2$ and then use the particular case formalism of Section III-C? In order to answer this question, we use MC simulations that were performed according to Section III-F1.

Afterward, we perform a histogram of these realizations and compare it first with the pdf obtained from the model without rotation, i.e., by using the $V\Gamma$ parameters of (13), and next with the pdf obtained from the model with rotation, i.e., by using the $V\Gamma$ parameters of (18). Fig. 3 shows an example of such a comparison. In this case ($\sigma_A^2 = 2$, $\sigma_B^2 = 1/2$, $\sigma_C^2 = 0$),

TABLE I
COMPARISON OF THE EXPECTED QUANTILES AND INTERVALS

Expected probabilities (%)	True probabilities (%)					
	Degrees of freedom: 2				dof: 8	
	$\sigma_C^2 = 0$					
	$\sigma_B^2 = 2$	1	2/3	1/2	0	0.5
Quantiles						
0.5	0.50	0.39	0.25	0.16	0.35	0.39
2.5	2.50	2.10	1.58	1.19	1.98	2.13
5.0	5.00	4.36	3.51	2.82	4.18	4.44
16.0	16.00	14.95	13.43	12.05	14.68	15.18
50.0	50.00	50.01	50.00	50.00	50.00	49.99
84.0	84.00	85.07	86.59	87.96	85.32	84.58
95.0	95.00	95.65	96.50	97.19	95.82	95.37
97.5	97.50	97.91	98.43	98.82	98.02	97.73
99.5	99.50	99.62	99.75	99.84	99.65	99.57
Intervals						
68.0	68.00	70.12	73.16	75.91	70.64	69.41
90.0	90.00	91.29	92.98	94.37	91.64	90.93
95.0	95.00	95.82	96.84	97.63	96.04	95.60
99.0	99.00	99.23	99.50	99.68	99.30	99.18

The expected quantiles (above) and intervals (below) are computed by using the parameters from Eq. (13) with empirical probabilities. For all realizations $\sigma_A^2 = 2$.

the pdf of the model with rotation is in perfect agreement with the histogram, whereas there are large discrepancies with the pdf of the model without rotation. We have thus a first result: the model without rotation should not be used when the ratio $\sigma_A^2/\sigma_B^2 \geq 4$.

To improve the efficiency of the test, we compute the theoretical quantiles by using the model without rotation and then deduce from them the theoretical confidence intervals that are often used (68%, 90%, 95%, and 99%). These quantiles and intervals are compared to the ones obtained from the simulation histogram. In one example of Table I, which corresponds to the case plotted in Fig. 3, the confidence intervals are strongly overestimated. For instance, the expected 68% confidence interval is significantly too large since it encompasses an interval of 76%. Similarly, the expected 90% interval is actually a 94% interval. This reinforces our decision of using the model with rotation for a noise variance ratio ≥ 4 .

We use these two approaches, i.e., pdf curve as well as confidence intervals, for many different parameter sets (see Table I). In any case, the agreement between the model with rotation and the MC simulation histograms were perfect since the residual deviations can be largely assumed to be due to the finite sample number of the simulation [less than 0.05% of the cumulative distribution function (CDF)]. However, this test is very interesting for the model without rotation since it allows us to answer the question which is the title of this section: when can the instrument noises be assumed to be “about the same”? Table I is very useful in this connection. In a first step, let us study the case where the number of DOF is 2 and there is no signal since it is the case that is the most sensitive to the difference between the noise levels. We can see on this table that the model without rotation is perfect when the two noise levels are equal ($\sigma_B^2 = 2$), fair when the ratio of the noise levels is equal to 2 ($\sigma_B^2 = 1$), at the limit of acceptance when the ratio is 3 but not suitable for a ratio ≥ 4 .

The other columns of Table I, obtained with eight DOFs and with $\sigma_C^2 = \sigma_A^2/4$, confirm that the model without rotation is acceptable when the ratio of the noise variances is equal to 2.

Then, we recommend using the vector rotation process if the ratio of the noise variance is greater than 2.

IV. INVERSE PROBLEM

A. Principle of the Method

The Bayesian statistician has to solve the inverse problem in order to define a confidence interval for the true variance σ_C^2 , given a set of measurements and *a priori* information. Thereby, the cross-spectrum measurement \hat{Z} is now fixed as well as the instrument noise levels σ_A^2 and σ_B^2 , whereas the signal true variance σ_C^2 appears as a random variable. According to the Bayes theorem, the *a posteriori* density of an unknown true value θ given the measurements, here the cross spectrum \hat{Z} , is

$$\begin{cases} p(\theta|\hat{Z}) \propto p(\hat{Z}|\theta) \cdot \pi(\theta) \\ \int_0^\infty p(\theta|\hat{Z})d\theta = 1 \end{cases} \quad (21)$$

where $\pi(\theta)$ is the *a priori* density, named prior, and $p(\hat{Z}|\theta)$ is the pdf that corresponds to (12) determined in the direct problem. It remains to determine the prior $\pi(\theta)$ (i.e., the pdf before any measurement) to compute the *a posteriori* density.

One of the main issues of Bayesian analysis concerns the choice of this prior. We have no *a priori* knowledge about the behavior of the parameter θ . A total ignorance of knowledge leads to a prior equal to θ^{-1} , which means that all orders of magnitudes have the same probability. The choice of θ is subject to discussion and the reader should refer to [36, Appendix B].

The quantity that can be actually measured is the sum of the signal and the measurement noise. Hence, the prior should be accordingly given as a function of this sum. In other words, it is not possible to have any information on a signal with a level much smaller than the measurement noise. Hence, choosing a prior function of $\sigma_N^2 + \sigma_C^2$ ensures that the corresponding magnitude order of σ_C^2 does not dominate the *a posteriori* probability distribution. The measurement noise level decreases as m^{-1} , according to [5, eq. (11)], when averaging over different spectra realizations m . Therefore, it should depend on the number of DOF $\nu = 2m$ (i.e., considering the real and imaginary parts). From these considerations, we choose the following prior according to Fig. 4:

$$\pi(\theta) = \frac{1}{\theta} = \frac{1}{\sigma_N^2/\nu + \sigma_C^2} \quad (22)$$

where $\sigma_N^2 = (\sigma_A^2 + \sigma_B^2)/2$ is the known, “not random” averaged noise level. Thus, a small level of σ_C^2 is distributed roughly uniformly on a linear scale and large values are distributed with equal probability for equal logarithmic intervals.

B. Check of the Posterior Probability Density Function

According to (20), for two DOFs or $m = 1$ spectrum average and the particular case $\sigma_A^2 = \sigma_B^2 = \sigma_N^2$, we know

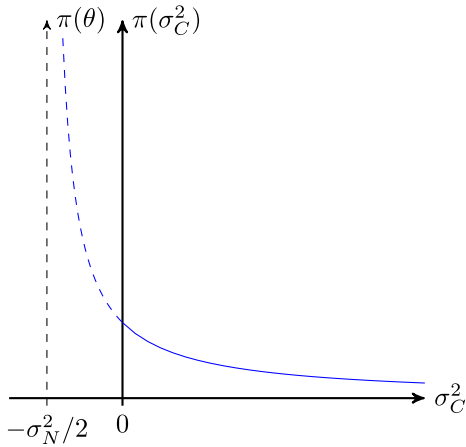


Fig. 4. Prior of the sum of the noise σ_N^2 and signal σ_C^2 levels for the case when there is no averaging spectra (i.e., $\nu = 2$).

that

$$p(\hat{Z}|\sigma_c^2) = \frac{e^{\hat{Z}/\sigma_N^2}}{2(\sigma_N^2 + \sigma_C^2)}.$$

Therefore, the posterior pdf of the cross-spectrum estimator is

$$\begin{cases} p(\sigma_C^2|\hat{Z}) \propto \frac{e^{\hat{Z}/\sigma_N^2}}{2(\sigma_N^2 + \sigma_C^2)(\sigma_N^2 + 2\sigma_C^2)} & \text{if } \hat{Z} \leq 0 \\ p(\sigma_C^2|\hat{Z}) \propto \frac{e^{-\hat{Z}/(\sigma_N^2 + 2\sigma_C^2)}}{2(\sigma_N^2 + \sigma_C^2)(\sigma_N^2 + 2\sigma_C^2)} & \text{if } \hat{Z} \geq 0. \end{cases} \quad (23)$$

We have checked this posterior pdf by using the inverse problem MC algorithm we already used in [28, Sec. IV.A.] and [31, Sec. IV.B.1)]. The principle is the following.

- S1: Select a target estimate $\hat{Z} = Z_0$.
 S2: Draw at random the signal level σ_C^2 according to

$$\sigma_C^2 = 10^{\lceil \eta + u_{[0,1]}(e^{\max} - \eta) \rceil} - \frac{\sigma_N^2}{2}$$

where $\eta = \log_{10}(\sigma_N^2/2)$ and $u_{[0,1]}$ is a pseudorandom function which is uniform within $[0, 1]$. This draw ensures that the parameter follows the prior of (22) up to $10^{e_{max}}$. We have chosen $e_{max} = 4$, which is in accordance with Fig. 4

- S3: Draw at random (Gaussian) the noise and signal estimates \hat{A} , \hat{B} , and \hat{C} and compute the measurements \hat{X} and \hat{Y} according to (8).
 S4: Compute the estimate \hat{Z} .
 S5: Compare the estimate \hat{Z} with the target Z_0 : if $\hat{Z} = Z_0 \pm p$, store the current σ_C^2 value as it is able to generate an estimate equal to the target; otherwise, throw this σ_C^2 value. We have chosen $p = (Z_0 + \sigma_N^2/2)/50$ when $Z_0 > 0$ and $p = \sigma_N^2/100$ when $Z_0 \leq 0$.
 S6: Go to step 2.
 S7: Stop when a set of 10000 σ_C^2 values is reached.

It must be noticed that such an algorithm is obviously not able to justify the choice of the prior since this prior is included in the algorithm. It will only ensure that no mistake has been done in the expression of the posterior pdf.

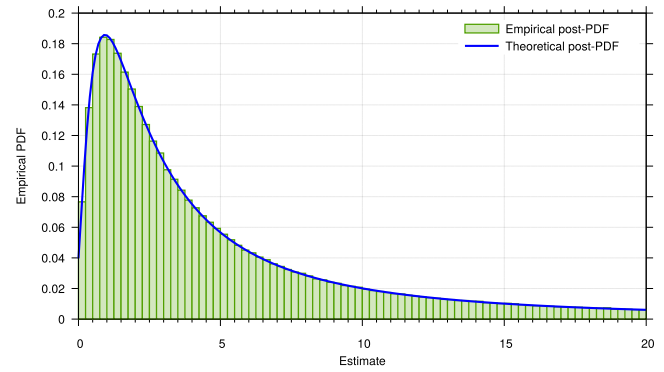


Fig. 5. Comparison of the empirical and theoretical posterior pdf for a noise level $\sigma_N^2 = 1$ a.u. and a target estimate $Z_0 = 1$ a.u.

TABLE II

COMPARISON OF THE QUANTILES 95% OBTAINED BY MC SIMULATION AND BY THE POSTERIOR CDF

Target Z_0 (a.u.)	95 % bound		True prob. (%)
	Emp	Theo	
-1.00	14.04	13.65	94.90
0.00	15.11	13.65	94.53
0.10	14.52	14.27	94.91
0.20	14.98	14.90	94.96
0.32	15.87	15.66	94.94
0.50	17.37	16.90	94.87
1.00	20.40	20.14	94.93
2.00	27.61	28.65	95.18
3.16	38.19	39.08	95.08
5.00	57.15	56.55	94.91
10.00	109.66	104.82	94.78

Fig. 5 shows the comparison of the posterior pdf computed according to (23) (blue curve) and the histogram obtained due to the inverse problem MC algorithm (green boxes) with a noise level $\sigma_N^2 = 1$ a.u. and a target estimate $Z_0 = 1$ a.u. We can verify that the agreement is excellent.

Table II compares the 95% quantiles obtained by the inverse problem MC algorithm (denoted “Emp” for empirical) and by the integration of the posterior pdf (denoted “Theo” for theoretical), i.e., the posterior CDF, for different values of target and for a noise level $\sigma_N^2 = 1$. Here, also, the agreement is very good whether for the 95% bounds or for the true probabilities of the theoretical bounds. Moreover, the fluctuations of the empirical bounds prove that the slight differences between the empirical and theoretical values are due to the fluctuations of the empirical bounds because of the limited number of realizations (10000) of the inverse problem MC algorithm.

C. KLT Method

The KLT method stands for “Karhunen–Loève transform” and was developed in our previous article [28]. In that article, KLT has proved to be as efficient as well as rigorous method, making the most of the property of “sufficient statistics.” However, the difference with [28] is that we do not have the “sufficient statistics” property (see [37]). It means that the KLT method will not give the same result as the cross-spectrum method, whereas it should have in the case of “sufficient statistics.” First, let us remind the theory. Then, in a second

time, we will explain what can bring the KLT method in addition to the cross-spectrum one.

1) *A Posteriori Distribution*: The KLT method relies on the use of \hat{X} and \hat{Y} measurements according to (2), which are Gaussian rv instead of the product of \widehat{AB} , \widehat{AC} , \widehat{BC} , and \widehat{C}^2 , which are a linear combination of Bessel of the second kind functions and χ^2 random variables. The main advantage of this approach lays in the property of the Gaussian rv, which remains Gaussian when they are linearly combined. However, these measurements are not independent. This is why we aim to determine two linear combinations of these rv that are independent of each other. Hence, we define the covariance matrix between \hat{X} and \hat{Y} given by

$$M = \begin{pmatrix} \sigma_A^2 + \sigma_C^2 & \sigma_C^2 \\ \sigma_C^2 & \sigma_B^2 + \sigma_C^2 \end{pmatrix}. \quad (24)$$

The KLT consists in using the rv corresponding to the diagonalization of this matrix. In order to simplify the equations, we study solely the case where $\sigma_A^2 = \sigma_B^2 = \sigma_N^2$. The eigenvalues of M are

$$\begin{aligned} \lambda_1 &= \sigma_N^2 + 2\sigma_C^2 \\ \lambda_2 &= \sigma_N^2 \end{aligned} \quad (25)$$

with the following normalized eigenvectors:

$$V_1 = \frac{1}{\sqrt{2}} \begin{pmatrix} 1 \\ 1 \end{pmatrix} \quad V_2 = \frac{1}{\sqrt{2}} \begin{pmatrix} 1 \\ -1 \end{pmatrix} \quad (26)$$

The likelihood function is then given by

$$p_{\text{KLT}}(\hat{Z}|\sigma_C^2) = \prod_{i=1}^2 \frac{1}{\lambda_i^{v/2}} \exp\left(-\frac{\sum_{j=1}^v \hat{w}_{i,j}^2}{2\lambda_i}\right). \quad (27)$$

The numerator of the exponential argument is then the only term that depends on the actual measurements

$$\hat{w}_{i,j}^2 = V_{i,1}^2 \hat{X}_j^2 + V_{i,2}^2 \hat{Y}_j^2 + 2V_{i,1}V_{i,2} \hat{Z}_j \quad (28)$$

where $\|V_i\|^2 = \sum_j V_{i,j}^2$. Therefore, the KLT method involve the spectral density \hat{X}^2 and \hat{Y}^2 in addition to the cross spectrum.

Keeping the same prior defined in (22), we have the following *a posteriori density*:

$$\begin{cases} p_{\text{KLT}}(\sigma_C^2|\hat{Z}) \propto \frac{1}{\sigma_N^2/2 + \sigma_C^2} \cdot p_{\text{KLT}}(\hat{Z}|\sigma_C^2) \\ \int_{\mathbb{R}} p_{\text{KLT}}(\sigma_C^2|\hat{Z}) d\sigma_C^2 = 1. \end{cases} \quad (29)$$

2) *Validation of the Method by Monte Carlo Simulation*: In order to validate the KLT method, we have compared its results to MC simulations. The algorithm is as follows.

S1: Select a noise level $\sigma_N^2 = \sigma_A^2 = \sigma_B^2$, a target $\hat{Z} = Z_0$, and a combination $\hat{X} = X_0$ and $\hat{Y} = Y_0 = Z_0/X_0$ for all the DOFs.

S2: Draw at random the signal level σ_C^2 according to

$$\sigma_C^2 = 10^{[\eta + u_{[0,1]}(e^{\max} - \eta)]} - \frac{\sigma_N^2}{2}$$

where $\eta = \log_{10}(\sigma_N^2/2)$ and $u_{[0,1]}$ is a pseudorandom function which is uniform within $[0, 1]$. This draw ensures

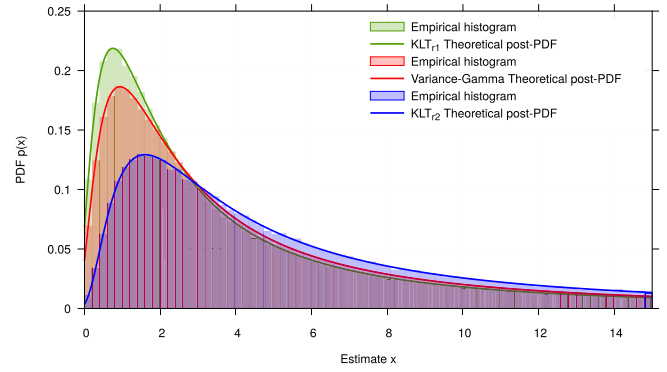


Fig. 6. Comparison of the empirical and theoretical posterior pdf for $V\Gamma$ and KLT methods with a noise level $\sigma_N^2 = 1$ a.u and a target estimate $Z_0 = 5$ a.u. KLT_{r1} and KLT_{r2} are the same method but differ by their combination of spectral density \hat{X}^2 and \hat{Y}^2 which are fixed (see Table III), whereas they are rv for the $V\Gamma$ method.

that the parameter follows the prior of (22) up to $10^{e_{\max}}$. We have chosen $e_{\max} = 4$.

S3: Draw at random (Gaussian) the noise and signal estimates \hat{A} , \hat{B} , and \hat{C} and compute the measurements \hat{X} and \hat{Y} according to (8).

S4: Compute the estimates \hat{X} and \hat{Y} .

S5: Compare the estimates \hat{X} and \hat{Y} with the targets X_0 and Y_0 for all the DOFs: if $\hat{X} = X_0 \pm p$, $\hat{Y} = Y_0 \pm q$, store the current σ_C^2 value as it is able to generate an estimate equal to the target; otherwise, throw this σ_C^2 value. We have chosen a precision p and q of tenths of, respectively, X_0 and Y_0 .

S6: Go to step 2.

S7: Stop when a set of n σ_C^2 values is reached. The number of values n depends on the computation time.

3) *Results and Discussion*: Fig. 6 shows the comparison between the pdf of $V\Gamma$ method developed in Section III and the pdf of KLT method for two different realizations. The theoretical post-pdf fits very well the empirical histogram for each method. The “sufficient statistics” property being not valid, different combinations of the spectral density \hat{X} and \hat{Y} were tested and are given in Table III. Indeed, KLT_{r1} and KLT_{r2} realizations do not give the same pdf unlike the $V\Gamma$ method. KLT_{r1} has then a peak that is higher than the $V\Gamma$ method, whereas KLT_{r2} has a smaller one. This is explained by a more stringent confidence interval for KLT_{r1} than $V\Gamma$ and a less stringent for KLT_{r2} as referred in Table III. The 95% quantiles obtained with MC simulations are in good agreement with the theoretical ones, especially for KLT_{r1} and $V\Gamma$ methods. It is explained by the number of data which is not the same for all of these simulations. $V\Gamma$, KLT_{r1} , and KLT_{r2} have, respectively, 1 000 000, 500 000, and 245 000 data. $V\Gamma$ MC simulations take only 2 min, whereas it needs, respectively, 54 h and 35 days using 17 cores, for KLT_{r1} and KLT_{r2} . KLT_{r1} is chosen to have the spectral density combination, which leads to the most stringent confidence interval, whereas KLT_{r2} is chosen to be more defavorable than the general case $V\Gamma$ using only the knowledge of the cross-spectrum measurement.

TABLE III

COMPARISON OF THE 95% QUANTILES OBTAINED BY MC SIMULATION (EMPIRICAL) AND BY THE POSTERIOR CDF

Method	Measurement				95 % bound	
	X'	X''	Y'	Y''	Emp	Theo
$V\Gamma$	rv	rv	rv	rv	56.4	56.6
KLT_{r-1}	1.6	1.6	1.6	1.6	48.4	48.3
KLT_{r-2}	4.0	0.6	2.5	1.0	82.3	80.8

The KLT method can then have a slightly more stringent confidence interval than the cross-spectrum method using $V\Gamma$ for a certain case. However, it requires having the knowledge of both the spectral densities of each channel. It then uses more information, the “sufficient statistics” property being not valid. Therefore, the KLT method is preferred when the spectral densities are known.

V. CONCLUSION

The method developed, $V\Gamma$, provides the pdf of the signal level studied when using the cross-spectrum method. It allows the determination of confidence intervals through numerical integration, where only the high bound has a physical meaning. It is especially relevant for one or several measurements of the cross-spectrum as the pdf will tend to a Gaussian distribution for many DOFs.

$V\Gamma$ is a rigorous method since it is the exact density solution of the cross-spectrum real part statistics, with no approximation. We shall notice that the noise level of each measurement instrument has to be known. If these noise levels are the same except at a factor of 4 and higher, we can assume that all the theoretical parts of orthogonalizing and the rotation of the basis are not necessary. This method works whatever the number of measurement spectra and noise level.

However, using the KLT method to compute the confidence interval is a more rigorous method because it uses the knowledge of the spectral density in addition to the cross spectrum. This is why we recommend using the KLT method, which turns out to be a slightly better estimator than $V\Gamma$.

REFERENCES

- [1] R. B. Blackman and J. W. Tuckey, *The Measurement of Power Spectra*. New York, NY, USA: Dover, 1959.
- [2] M. Gwilym Jenkins and G. Donald Watts, *Spectral Analysis and its Applications*. San Francisco, CA, USA: Holden Day, 1968.
- [3] O. E. Brigham, *The Fast Fourier Transform and its Applications*. Upper Saddle River, NJ, USA: Prentice-Hall, 1988.
- [4] D. B. Percival and A. T. Walden, *Spectral Analysis for Physical Applications*. Cambridge, U.K.: Cambridge, 1993.
- [5] E. Rubiola and F. Vernotte, “The cross-spectrum experimental method,” 2010, *arXiv:1003.0113*. [Online]. Available: <http://arxiv.org/abs/1003.0113>
- [6] R. H. Dicke, “The measurement of thermal radiation at microwave frequencies,” *Rev. Sci. Instrum.*, vol. 17, no. 7, pp. 268–275, Jul. 1946.
- [7] M. Sampietro, L. Fasoli, and G. Ferrari, “Spectrum analyzer with noise reduction by cross-correlation technique on two channels,” *Rev. Sci. Instrum.*, vol. 70, no. 5, pp. 2520–2525, May 1999.
- [8] A. Hati, C. W. Nelson, and D. A. Howe, “Cross-spectrum measurement of thermal-noise limited oscillators,” *Rev. Sci. Instrum.*, vol. 87, no. 3, Mar. 2016, Art. no. 034708.
- [9] Y. Gruson, V. Giordano, U. L. Rohde, A. K. Poddar, and E. Rubiola, “Cross-spectrum PM noise measurement, thermal energy, and metamaterial filters,” *IEEE Trans. Ultrason., Ferroelectr., Freq. Control*, vol. 64, no. 3, pp. 634–642, Mar. 2017.

- [10] A. C. Cárdenas-Olaya, R. Friedt and P.-Y. Calosso, “Noise characterization of analog to digital converters for amplitude and phase noise measurements,” *Rev. Sci. Instrum.*, vol. 88, Jun. 2017, Art. no. 0651081.
- [11] G. Feldhaus and A. Roth, “A 1 MHz to 50 GHz direct down-conversion phase noise analyzer with cross-correlation,” in *Proc. Europ. Freq. Time Forum*, New York, NY, Apr. 2016, pp. 1–4.
- [12] T. M. Fortier *et al.*, “Sub-femtosecond absolute timing jitter with a 10 GHz hybrid photonic-microwave oscillator,” *Appl. Phys. Lett.*, vol. 100, Jun. 2012, Art. no. 2311111.
- [13] E. Rubiola, “The measurement of AM noise of oscillators,” Dec. 2005, *arXiv:physics/0512082*. [Online]. Available: <http://arxiv.org/abs/physics/0512082>
- [14] A. H. Verbruggen, H. Stoll, K. Heeck, and R. H. Koch, “A novel technique for measuring resistance fluctuations independently of background noise,” *Appl. Phys. A, Solids Surf.*, vol. 48, pp. 233–236, Mar. 1989.
- [15] C. M. Allred, “A precision noise spectral density comparator,” *J. Res.*, vol. 66, pp. 323–330, Oct./Dec. 1962.
- [16] J. A. Nanzer and R. L. Rogers, “Applying millimeter-wave correlation radiometry to the detection of self-luminous objects at close range,” *IEEE Trans. Microw. Theory Tech.*, vol. 56, no. 9, pp. 2054–2061, Sep. 2008.
- [17] D. R. White *et al.*, “The status of Johnson noise thermometry,” *Metrologia*, vol. 33, no. 4, pp. 325–335, Aug. 1996.
- [18] J. P. W. Verbiest *et al.*, “Timing stability of millisecond pulsars and prospects for gravitational-wave detection,” *Monthly Notices Roy. Astronomical Soc.*, vol. 400, no. 2, pp. 951–968, Dec. 2009.
- [19] S. Detweiler, “Pulsar timing measurements and the search for gravitational waves,” *Amer. Astronom. Soc.*, vol. 234, pp. 1100–1104, Dec. 1979.
- [20] R. W. Hellings and G. S. Downs, “Upper limits on the isotropic gravitational radiation background from pulsar timing analysis,” *Amer. Astronom. Soc.*, vol. 265, pp. 39–42, Feb. 1983.
- [21] S. R. Taylor, M. Vallisneri, J. A. Ellis, C. M. F. Mingarelli, T. J. W. Lazio, and R. V. Haasteren, “Are we there yet? Time to detection of nanohertz gravitational waves based on pulsar-timing array limits,” *Astrophys. J.*, vol. 819, no. 1, p. L6, Feb. 2016.
- [22] D. Perrodin and A. Sesana, *Radio Pulsars: Testing Gravity and Detecting Gravitational Waves*, vol. 425. Cham, Switzerland: Springer, 2018.
- [23] S. Drasco and E. E. Flanagan, “Detection methods for non-Gaussian gravitational wave stochastic backgrounds,” *Phys. Rev. D, Part. Fields*, vol. 67, no. 8, 2003, Art. no. 082003.
- [24] N. J. Cornish and J. D. Romano, “Towards a unified treatment of gravitational-wave data analysis,” *Phys. Rev. D, Part. Fields*, vol. 87, no. 12, Jun. 2013, Art. no. 122003.
- [25] C. G. Bassa *et al.*, “Leap: The large European array for pulsars,” *Month. Not. Roy. Astronom. Soc.*, vol. 456, no. 2, pp. 2196–2209, Dec. 2015.
- [26] S. Chen, F. Vernotte, and E. Rubiola, “Applying clock comparison methods to pulsar timing observations,” in *Proc. MNRAS*, 2020.
- [27] *International Vocabulary of Basic and General Terms in Metrology (VIM)*, International Organization for Standardization (ISO), Geneva, Switzerland, 2004.
- [28] E. Lantz *et al.*, “KLTS: A rigorous method to compute the confidence intervals for the three-cornered hat and for gros Lambert covariance,” *IEEE Trans. Ultrason., Ferroelectr., Freq. Control*, vol. 66, no. 12, pp. 1942–1949, Dec. 2019.
- [29] N. J. Kasdin, “Discrete simulation of colored noise and stochastic processes and $1/f^2$ power law noise generation,” *Proc. IEEE*, vol. 83, no. 5, pp. 802–827, May 1995.
- [30] F. Vernotte, G. Zalamansky, and E. Lantz, “Time stability characterization and spectral aliasing. Part I: A time-domain approach,” *Metrologia*, vol. 35, no. 5, pp. 723–730, Oct. 1998.
- [31] F. Vernotte and E. Lantz, “Three-cornered hat and Gros Lambert covariance: A first attempt to assess the uncertainty domains,” *IEEE Trans. Ultrason., Ferroelectr., Freq. Control*, vol. 66, no. 3, pp. 643–653, Mar. 2019.
- [32] M. Haas and C. Pigorsch, *Financial Economics, Fat-Tailed Distributions*. New York, NY, USA: Springer, 2009, pp. 3404–3435.
- [33] B. Sorin and P. Thionet, “Lois de probabilités de Bessel,” *Rev. Stat. App.*, vol. 16, no. 4, pp. 65–72, 1968.
- [34] D. Madan and E. Seneta, “The variance gamma (V.G.) model for share market returns,” *J. Bus.*, vol. 63, no. 4, pp. 511–524, 1990.
- [35] G. N. Watson, *A Treatise Theory Bessel Functions*. Cambridge, U.K.: Cambridge Univ. Press, 1922.
- [36] M. P. McHugh, G. Zalamansky, F. Vernotte, and E. Lantz, “Pulsar timing and the upper limits on a gravitational wave background: A Bayesian approach,” *Phys. Rev. D, Part. Fields*, vol. 54, no. 10, pp. 5993–6000, Nov. 1996.
- [37] G. Saporta, *Probabilités, Analyse des données et Statistique*. London, U.K.: Technip, 1990.